Control Co-Design of 13 MW Downwind Two-Bladed Rotors to Achieve 25% Reduction in Levelized Cost of Wind Energy

Lucy Y. Pao[a,*], Daniel S. Zalkind[a], D. Todd Griffith[b], Mayank Chetan[b], Michael S. Selig[c], Gavin K. Ananda[c], Christopher J. Bay[d], Tyler Stehly[d], Eric Loth[e]

[a]*Department of Electrical, Computer & Energy Engineering, University of Colorado, Boulder, CO 80309 USA*
[b]*Department of Mechanical Engineering, University of Texas at Dallas, Richardson, TX 75080 USA*
[c]*Department of Aerospace Engineering, University of Illinois at Urbana-Champaign, Champaign, IL 61820 USA*
[d]*National Wind Technology Center, National Renewable Energy Laboratory, Golden, CO 80401 USA*
[e]*Department of Mechanical and Aerospace Engineering, University of Virginia, Charlottesville, VA 22904 USA*

Abstract

Wind energy is recognized worldwide as cost-effective and environmentally friendly and is among the fastest-growing sources of electrical energy. To further decrease the cost of wind energy, wind turbines are being designed at ever larger scales, which is challenging due to greater structural loads and deflections. Large-scale systems such as modern wind turbines increasingly require a control co-design approach, whereby the system design and control design are performed in a more integrated fashion. We overview a two-bladed downwind morphing rotor concept that is expected to lower the cost of energy at wind turbine sizes beyond 13 megawatts (MW) compared with continued upscaling of traditional three-bladed upwind rotor designs. We describe an aero-structural-control co-design process that we have used in designing such extreme-scale wind turbines, and we discuss how we were able to achieve a 25% reduction in levelized cost of energy for our final turbine design compared to a conventional upwind three-bladed rotor design.

Keywords: wind energy, control co-design, aerodynamics, structural dynamics, cost of energy

1. Introduction

Development of the vast offshore wind resource, in the US and world-wide, is motivated by many attractive characteristics. However, there are also significant challenges – both technical and economic in nature. Opportunities in offshore wind include proximity to major population centers, stronger more consistent wind resources in comparison to those on land, a vast resource, and the ability to scale-up to larger turbine sizes with fewer logistical barriers. However, the challenges of offshore wind include high levelized cost of energy (LCOE) (in particular from higher balance of system costs related to offshore-specific infrastructure), accessibility for installation and maintenance, hurricanes, and in general inexperience [1, 2].

Large wind turbines have specific challenges and opportunities. Challenges of upscaling the turbine size include the "squared-cubed" law (energy capture versus capital costs) [3], technical and economic constraints of transportation, logistics (including installation, assembly, and manufacturing), and accessibility for inspection and maintenance. Specific structural design challenges for the composite rotor blades include strength, blade tip deflection, fatigue, panel buckling, and aero-elastic instability (e.g., flutter) [4, 5, 6]. However, there are many opportunities with larger machines including improved aerodynamics (high Reynolds number effects) and potential for "economies of scale" (reduced project costs per installed megawatt (MW)), which can yield LCOE reductions. In addition, there is an opportunity for completely new rotor / turbine design pathways leading to significant cost reduction.

Because of the opportunities noted above, larger and larger wind turbines are being installed offshore. The current state of the art for large wind turbines is in the range of 6 to 9.5 MW for rated power and 70 to 90 meters for blade length [7, 8]. Further, wind turbines in the 10 to 15 MW range with blades up to 108 meters are planned to be in commercial operation by 2022 to 2024 [9, 10]. Figure 1 provides a historical snapshot of blade size where 9-meter blades were prevalent in the late 1970s and early 1980s. Sixty-meter blades have been commonly installed offshore starting around 2010, and 100-meter blades for 10 to 13 MW machines are expected to be installed in the near future.

Wind turbines have traditionally been designed in a sequential process with the aerodynamical design of the rotor completed first, followed by the structural design that includes the detailed layup of materials to be used in manufacturing the blades. Usually, by the time the control systems engineers are requested to design and tune the

---

*Corresponding author
 Email address:* pao@colorado.edu (Lucy Y. Pao)

Figure 1: Blade size evolution over past 40 years and future envisioned extreme-scale rotors.

controllers, the wind turbine has already been completely designed [11]. Co-design methods that simultaneously optimize the system and the control design have been shown to yield superior results [11, 12, 13, 14]. Because of the complexity of the wind turbine design process, with numerous parameters that must be determined, and where it is not clear how certain parameters depend upon others, a fully simultaneous optimization of the physical wind turbine and control design parameters is not currently possible. Even when parameter dependencies become better understood, simultaneous optimizations would be extremely computationally intensive for wind turbine design. Given the presently available software tools, we have used an iterative sequential co-design process [15, 16] as a practical and beneficial approach for applying co-design to wind turbines. In contrast to simultaneous co-design where both the wind turbine and controller are simultaneously designed to minimize some cost function (such as LCOE), in each iteration of an iterative sequential co-design process the wind turbine is first designed to optimize one measure (such as minimizing mass subject to structural stability constraints) and then the controller is designed to optimize another function (such as maximizing annual energy production (AEP) subject to generator overspeed constraints). Each iteration makes use of performance measures (mass, structural loads, AEP, LCOE) from previous iterations to try to achieve improved performance measures.

In this paper, a new rotor design pathway based on iterative sequential control co-design is explored to achieve the envisioned benefits enabled by an extreme-scale rotor with blade lengths ranging from 100 to 150 meters. Aero-structural (AS) co-design has previously been used to design a conventional 3-bladed upwind rotor at the 13.2 MW scale (CONR-13) [17]. As wind turbines become larger, however, conventional upwind blade designs may be reaching a size limit because they must be designed to be massive and stiff enough to avoid tower strikes, even in extreme wind conditions.

For 13 MW or larger turbines, a downwind configuration can decrease the structural loads by allowing alignment of the net centrifugal, gravitational, and thrust force along the rotor blade. Such a downwind aligned configuration also increases the rated clearance distance between the rotor and the tower because wind loads push the blades further from the tower. Moreover, less massive blades could be used in such designs, leading to lower capital costs. Initial designs of this novel 2-bladed downwind segmented ultralight morphing rotor (SUMR-13i)

concept at the 13 MW scale have been documented in [18, 19, 20, 21, 22].

The current article provides an overview of an aero-structural-control co-design process that we have used to achieve a SUMR-13 design that has an LCOE which is 25% lower than that of the CONR-13 design. Within this large overall team project, our initial goal was to reduce rotor mass by 25%, which we achieved at the end of the first year of the project (with the SUMR-13A to be discussed further in Section 5.1). Our second-year goal was then to reduce LCOE by 25%. After realizing that 25% rotor mass reduction reduced the LCOE by only about 7% (which is later shown in Figure 12(d)), we then used a control co-design approach, which led us to longer blades as the best approach to minimize LCOE, and this blade length increase was enabled by the downwind SUMR design but was not the obvious initial solution.

The aim of this paper is to outline the overall control co-design process and to discuss how we have successfully used this procedure to attain a SUMR-13 design with significant LCOE reductions; throughout, we cite more focused disciplinary papers that provide further details on particular steps in the process. Our results show that increasing rotor sizes with the same generator rating is beneficial for reducing LCOE. Further, we find that lower axial induction rotors with longer and more slender blades are able to provide increases in AEP while not leading to increased structural loads. Lower axial induction and larger rotor sizes both lead to lower specific power, which is a trend [23] seen in industry because it reduces LCOE.

This article is organized as follows. Section 2 reviews the major wind turbine components as well as the CONR-13 design, and Section 3 describes the new SUMR concept. Section 4 outlines the iterative aero-structural-control co-design process, including defining how LCOE is computed. Our use of the process to iteratively design the SUMR-13 to reduce LCOE is documented in Section 5. Finally, conclusions and a discussion of future work is given in Section 6.

2. Conventional 13 MW 3-Bladed Upwind Rotor (CONR-13)

Figure 2 reviews the major wind turbine components. In designing wind turbines, it is necessary to determine the geometry and outer shape of the blades, the dimensions of the spar caps, shear webs, any leading edge and trailing edge reinforcements, as well as the detailed material layup for each component. Additional design variables include
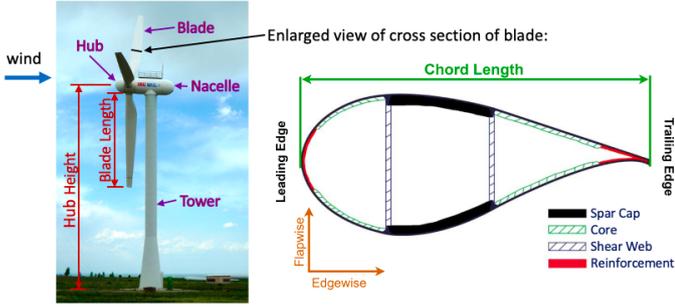
Figure 2: The major components of an (upwind) wind turbine (left) and of each blade (right). The wind turbine rotor consists of the hub and the blades. [Left photo courtesy of L. Fingersh.]
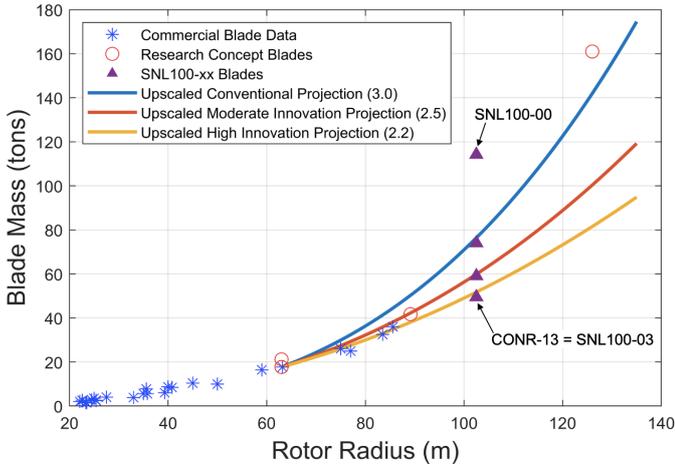

Figure 3: Blade mass trends with rotor size. The rotor radius is defined as the distance from the hub center to the end of the blade tip.
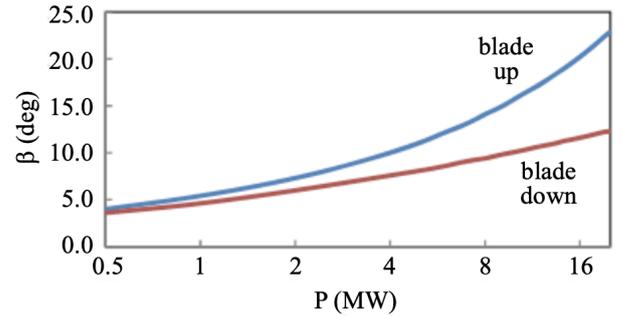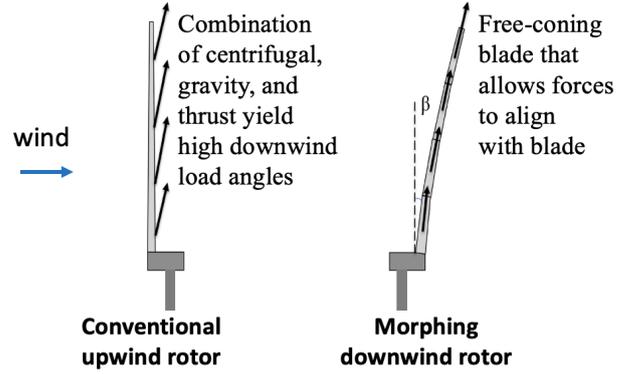

Figure 4: (top left) The non-torque forces on an upwind rotor blade yield downwind loads while (top right) a downwind rotor blade with complete load-alignment can eliminate these steady-state loads. (bottom) The span-averaged rated load-path angles for a downwind rotor at rated conditions (for when the blade is pointing upward and pointing downward relative to the ground) as a function of rated turbine power, showing potential benefits for load-alignment (complete or even partial) are much greater at extreme scales (>10 MW).

the shaft tilt and teeter hinge. Shaft tilt is the angle of the axis about which the rotor spins, measured with respect to horizontal; the upwind rotor on the left of Figure 2 has a small positive shaft tilt such that the rotor is looking slightly upward toward the sky. A hub with a teeter pivot point allows the rotor to pivot back and forth as forces change across the rotor; the design of the teeter hinge must account for friction, damping, and end stops [24].

The baseline design which we call CONR-13 was based on the SNL100-03 rotor design [17] for a 13.2 MW turbine, which has some of its properties upscaled from the NREL 5 MW research wind turbine [25]. Aero-structural co-design was used to reduce the mass from an initial all-glass design (SNL100-00) [3] by over 50% along the generations of the SNL100 series [17]. At the end of a series of studies investigating advanced core materials and flatback airfoils, the final design known as the SNL100-03 in [17] is a lightweight design for a 3-bladed upwind turbine. This design has a blade mass below the projected mass for an innovative 100-meter blade as shown in Figure 3. An important feature is that the SNL100-03 was designed with an integrated aerodynamic-structural design process whereby the blade external geometry (the aerodynamic definition

of airfoil placement, chord, and twist) was designed with structural constraints to develop a blade that provided the best trade-offs in aerodynamic and structural performance. This approach resulted in a very lightweight design for the SNL100-03. The current work expands the scope to a multi-disciplinary aeroelastic-structural-control co-design process to successfully develop a 13.2 MW wind turbine rotor with dramatic LCOE reduction relative to the SNL100-03, which we will refer to in the remainder of this paper as the CONR-13 rotor.

3. SUMR concept

The proposed wind turbine concept is bio-inspired by palm trees, which can withstand high-speed winds through aeroelastic adaptivity. In particular, the palm tree trunk is reasonably stiff in moderate winds but bends to align itself in high winds. This natural adaptability of the trunk thus handles extreme aerodynamic loads with minimal structural mass. For a wind turbine, a downwind design coupled with downwind coning to align with the steady-state flapwise forces at rated conditions (Figure 4 top right) can dramatically reduce cantilever loads. This concept is termed a pre-aligned rotor because it is effectively a rigid coned

3

rotor at the hub with an aeroelastically-induced down-wind curvature along the blades to minimize stress near the rated conditions. This concept extends previous work in [26, 27, 28] for small-scale and conventional-scale systems (< 5 MW) for which the load-alignment angles are modest. In particular, turbines with ratings of less than 1 MW typically have rated load-path angles of less than 5° (Figure 4 bottom). As such, an upwind conventional rotor can reasonably accommodate this load-path through a combination of structural stiffness, upwind pre-cone, and shaft tilt.

This load-alignment concept becomes more important for extreme-scale systems (greater than 10 MW rated power) since the load angles become much larger (Figure 4 bottom) [29, 30]. This increase occurs because the ratio of thrust forces/moments relative to centrifugal forces/moments tends to scale nearly linearly with rated power once we consider technology advancements associated with blade length increases [31]. Similarly, the gravity-induced load angle differences (as a function of azimuthal angle) also increase as rated power increases. Therefore, flapwise mean and fluctuating moments become more and more problematic for a conventional upwind turbine, requiring extra blade structural mass and pre-cone to avoid tower strike. By shifting to a downwind coned turbine, pre-alignment combined with teeter or individual pitch control can eliminate the quasi-steady flapwise moments for a specified wind speed and operational condition. However, it should be noted that this alignment will not generally hold at other wind speeds.

Furthermore, fluctuations in flapwise moments due to turbulence are generally significant. As a result, variable speed and variable pitch control strategies are often needed to accommodate rapid changes in wind angle or speed caused by gusts [32, 33]. Downwind alignment can only reduce (not eliminate) flapwise bending moments. By mitigating these bending moments, however, there is an opportunity to improve upon the turbine performance by either reducing overall rotor mass (to help reduce capital costs) or by increasing rotor diameter (to help increase annual energy capture).

4. Iterative Aero-Structural-Control Co-Design Process

Our vision of the iterative wind turbine co-design process is shown in Figure 5, where we begin with an initial aerodynamic and structural design model that is translated into a wind turbine simulation model in an aeroelastic software tool such as FAST [34]. A controller is required to evaluate simulations defined in design load cases (DLCs) specified by the International Electrotechnical Commission (IEC) [4]; this is discussed further in Section 4.1. Because currently available software tools (to be discussed further in Section 4.3) are not yet well integrated, we are not able to do a simultaneous optimization of controller parameters along with the turbine parameters. Rather,
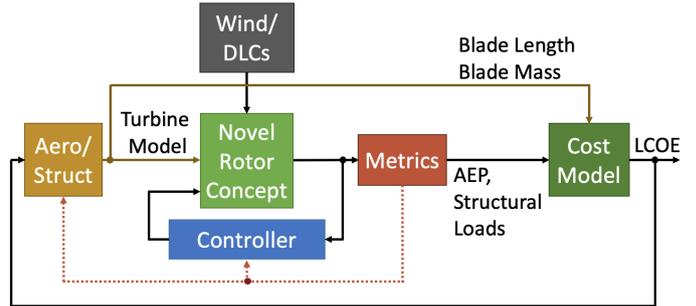

Figure 5: Block diagram illustrating our integrated wind turbine design process, which we applied in multiple design iterations on the novel SUMR concept to reduce the LCOE relative to the CONR-13.

the feedback paths shown in Figure 5 indicate that various performance measures (such as AEP and structural loads) from the results of the DLC simulations are fedback so that the wind turbine and controller designs can be refined to improve upon these metrics. The form of the controller used (discussed further in Section 4.3.2) is similar to what we believe to be the industry standard [25, 35, 36]. While the form of the controller does not change from one iteration to the next, the controller parameters must be re-tuned and optimized for each new wind turbine design.

As indicated in Figure 5, wind turbine model parameters and performance metrics are used in cost models that determine the LCOE, which we describe in Section 4.2. Information from the cost analysis is then used in subsequent design cycle iterations until a sufficiently optimized wind turbine design is achieved that meets cost objectives. Our aim in this study was to achieve a SUMR-13 design with an LCOE that is 25% lower than the LCOE of the CONR-13 design.

After discussing DLCs and LCOE further in Sections 4.1 and 4.2, we walk through a single design iteration in more detail in Section 4.3 and describe the interaction between the aerodynamic, structural, and control design aspects.

4.1. Design load cases (DLCs)

IEC standards [4] specify DLCs that define the minimum conditions a wind turbine structure must survive, including different levels of turbulence for fatigue and extreme loads, extreme wind events, fault conditions, shutdown procedures, and parked conditions. The DLC with the greatest load on a hardware component, e.g., the blade, is referred to as the design-driving load case for that component. Sometimes, the design driving load case is a fault case, where torque or pitch control actuation is lost. The type of faults simulated and the manner in which fault cases are handled is manufacturer specific. Thus, for research purposes, we focus on more general DLCs; in our design process, we evaluate the SUMR rotors for the DLCs in Table 1.

Design optimizations discussed in [37] pre-compute extreme loads from simulations and use estimates of fatigue loading. These loads are used as constraints to optimize

Table 1: Selected Design Load Cases (DLCs) from [4] used to constrain the fatigue and extreme loads on the blades of the SUMR rotor

DLC	Description	Fatigue/Extreme
1.2	Normal turbulence	Fatigue
1.3	Extreme turbulence	Extreme
1.4	Extreme coherent gust with direction change	Extreme
1.5	Extreme wind shear	Extreme
5.1	Shutdown in normal turbulence	Extreme
6.1	Parked in a 50-year wind speed	Extreme

the aerodynamic and structural blade design, but this limits significant changes to the rotor and controller, which can affect the design loads. Before finalizing a design, the loads during each of these DLCs must be simulated using an aeroelastic wind turbine code like FAST [34].

By incorporating closed-loop simulations in the wind turbine design loop, more drastic changes to the rotor can be analyzed and the effects of control, like load reduction, optimal tuning, and power boosting can be used *during* the design process. In this project, we have designed several controllers for fatigue and extreme load reduction, which can reduce the structural loads in design-driving load cases of a rotor, yielding a more optimal design. Conducting closed-loop simulations for design iterations results in a large computational expense, but have begun to be used in more recent holistic design optimizations [38]. We will outline tools that have been developed to reduce the computational expense of performing these closed-loop simulations, which can be used to estimate load limits and power capture.

Ultimately, the cost of the turbine components ($CapEx$) must be compared with the power capture (or AEP) to determine the LCOE for the wind turbine. The wind farm site conditions often determine whether it may be more favorable to reduce $CapEx$ versus increasing power capture. For offshore sites, where installation and substructure costs are high, designs are typically aimed at increasing power capture using larger rotors. Recent design optimizations [38] and industry trends [7, 8, 9, 10] have reflected this rotor upscaling trend. The remainder of this article outlines how drastic changes in rotor size have affected power capture and cost of energy in our control co-design iterations. In particular, we compare 2-bladed downwind SUMR rotor designs with a conventional 3-bladed (CONR-13) upwind rotor design, as depicted in Figure 6.

4.2. Levelized cost of energy (LCOE)

In order to compare the cost of various energy sources, a metric that has seen widespread use is LCOE, which includes the cost of electricity generation and the plant-level impact of design changes. The method of LCOE presented here is based on the definition given in [2]. LCOE (in $/kWh) is computed as

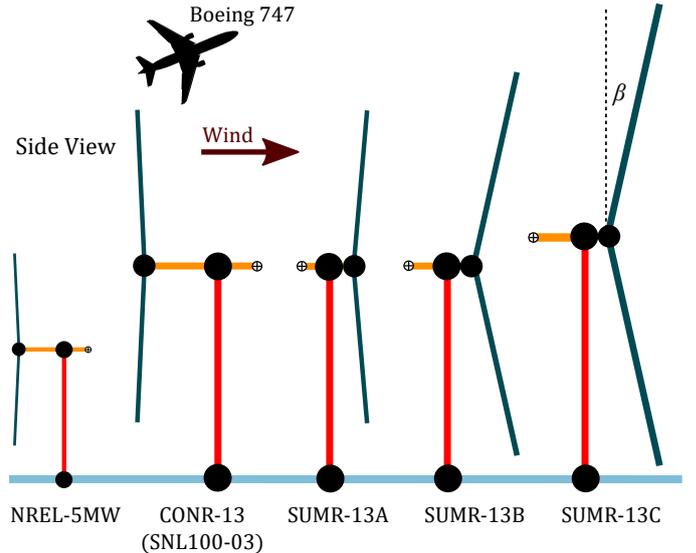$$\text{LCOE} = \frac{(CapEx \cdot FCR) + OpEx}{AEP_{net}} \quad (1)$$

Figure 6: Diagrams of the turbines designed and analyzed in this study, along with the NREL-5MW reference turbine [25] for comparison. Tower heights, rotor radii, and cone angles (β) are drawn to scale; overhangs and nacelle center-of-masses are enlarged for comparison.

where $CapEx$ represents the Capital Expenditures [$/kW], FCR is the Fixed Charge Rate [%/yr] (incorporating financing costs), $OpEx$ represents the Operational Expenditures [$/kW/yr], and AEP_{net} is the net average Annual Energy Production per rated power [MWh/MW/yr].

$CapEx$ includes several parts. One component is the turbine cost, including rotor, nacelle, and tower costs. Another component is the Balance of System (BOS) cost, which includes assembly and installation, electrical infrastructure, the turbine substructure, and the foundation for fixed-bottom turbines. A third major component of $CapEx$ is the financing cost, including construction finance, contingency funds, and decommissioning. The Fixed Charge Rate (FCR) is the amount of revenue required to pay the annual carrying charges that are applied to the $CapEx$ for the economic life of the wind plant [39]. The FCR essentially annualizes the capital costs of the project over the lifetime of the plant, allowing for a straight-forward inclusion of capital costs in the LCOE.

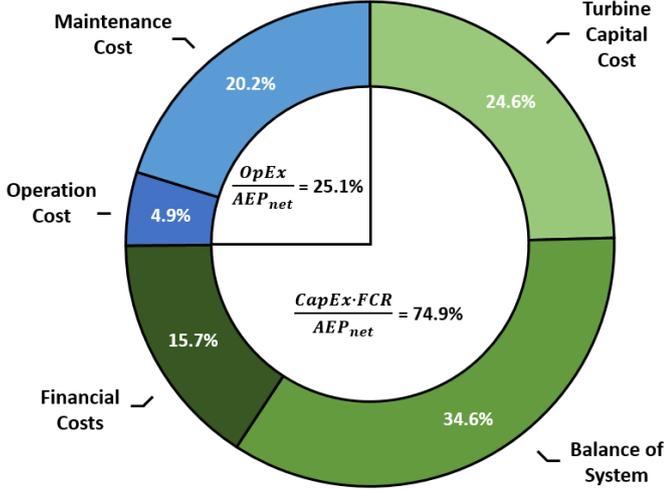$OpEx$ is made up of two significant costs: maintenance

Figure 7: Breakdown of Capital Expenditures ($CapEx$) and Operational Expenditures ($OpEx$) as a percentage of Levelized Cost of Energy (LCOE) for offshore, fixed-bottom wind plants based on data from [2].

and operation. Both are greatly affected by the distance of the wind plant from the required maintenance resources as well as the ocean climate at the site. Weather results in limited windows during which repairs/maintenance can occur.

Lastly, AEP_{net} represents the net annual energy production of the wind plant and accounts for the available wind resource based on the site and losses due to wind plant layout, energy conversion efficiency, and transmission of the energy. When we refer to AEP by itself (as done in the next subsection), it does not account for these losses.

For offshore, fixed-bottom wind plants, $CapEx$ accounts for approximately 75% of LCOE for the turbines that were surveyed in [2], as shown in Figure 7. $OpEx$ accounts for the other 25%. Reductions in both $CapEx$ and $OpEx$ will help reduce the overall LCOE for offshore wind energy, but referring to Eq. (1), we can see that increases to AEP_{net} offset both $CapEx$ and $OpEx$ to give a lower LCOE. It is this realization that drove our SUMR wind turbine design iterations, as explained in later sections.

We used detailed cost models to compute accurate LCOE values for the CONR-13 as well as for our final SUMR-13C design (to be discussed further in Section 5.3). The $OpEx$ for the CONR-13 and SUMR-13C scenarios were estimated using the ECN O&M tool v.4 software [40]. A number of differences between the CONR-13 and SUMR-13C scenarios were assumed for the cost model runs. These include, but are not limited to, differences in the number of site visits for blade inspections (i.e., different number of blades within the wind plants, assuming similar plant size), failure frequencies of components (e.g., additional use of pitch actuation for advanced controls), and the size of equipment used for blade repairs (i.e., larger capacity equipment for larger blades). The es-

timated $OpEx$ from the ECN tool resulted in about a 7% increase for SUMR-13C when compared to CONR-13.

The SUMR-13 blades were designed to meet the DLCs and the reliability of the rotors were evaluated to have similar lifetimes [22] hence not measurably affecting the $OpEx$ calculations across different SUMR-13 rotor designs. While structural loading does vary across different SUMR-13 designs (as will be shown in Figure 13), since there is very little field data that shows clear trends on how structural loads affect $OpEx$ in general [41], these are not usually accounted for in the $OpEx$ calculations.

4.2.1. A simplified LCOE analysis for design iteration

In order to expedite our design iterations, we used a simplified method for computing the relative LCOE for the intermediate SUMR models as we progressed through our overall study. The simplified model starts with an established design (the CONR-13) and its known cost breakdown, which is similar to that in Figure 7. The total cost is comprised of

$$C_{\text{Tot}} = (CapEx \cdot FCR) + OpEx, \tag{2}$$

where $(CapEx \cdot FCR) = C_{\text{Turb}} + C_{\text{BOS}} + C_{\text{Fin}}$. Financial costs, C_{Fin}, depend on the FCR as well as on economic markets and policy. C_{BOS} is the BOS costs, and the portion that includes the turbine parts, C_{Turb}, can be further subdivided into

$$C_{\text{Turb}} = C_{\text{Rot}} + C_{\text{Nac}} + C_{\text{Twr}}, \tag{3}$$

where C_{Rot} is the rotor cost, including blades, hub, and pitch actuators, C_{Nac} is the nacelle cost, including the generator, main bearing, gearbox, and bedplate, and C_{Twr} is the cost of the tower. Determining the actual cost figures for each of these terms is a detailed and extensive process that can be aided by using system engineering tools.

For simplicity, we assume that C_{Rot} is the rotor cost of the CONR-13 and other costs are constant for all models. We also assume that blade mass is directly related to the new rotor cost

$$C'_{\text{Rot}} = \frac{m'_b}{m_b} C_{\text{Rot}}, \tag{4}$$

where m'_b is the combined mass of the new blades, and m_b is the combined mass of the blades of CONR-13 design. We assume that the other rotor components do not have any change in cost, so the updated turbine cost is

$$C'_{\text{Turb}} = C'_{\text{Rot}} + C_{\text{Nac}} + C_{\text{Twr}} \tag{5}$$

and the updated total cost is

$$C'_{\text{Tot}} = C'_{\text{Turb}} + C_{\text{BOS}} + C_{\text{Fin}} + OpEx. \tag{6}$$

Thus, the updated LCOE, including the new AEP (AEP') is

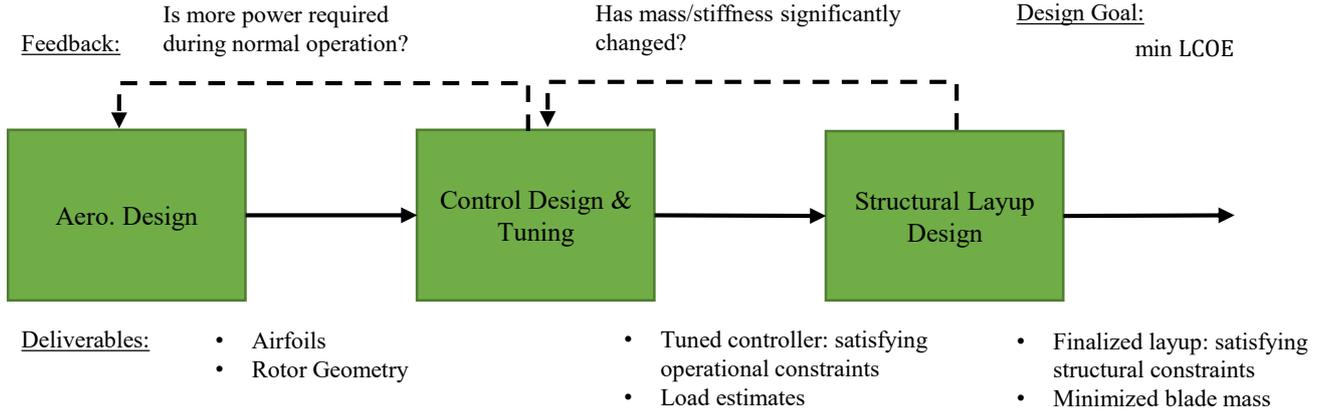$$\text{LCOE}' = \frac{C'_{\text{Tot}}}{AEP'}. \tag{7}$$

Figure 8: A single rotor design iteration, detailing the coordination among the aerodynamics, controls, and structures teams.

Compared to the original LCOE, we can determine the relative change by

$$\frac{\text{LCOE}'}{\text{LCOE}} = \left(\frac{C'_{\text{Tot}}}{C_{\text{Tot}}}\right)\left(\frac{AEP}{AEP'}\right). \tag{8}$$

While the simplified LCOE computations for intermediate SUMR designs (to be discussed in Section 5) used the $OpEx$ that was computed for the CONR-13 in (6), as indicated in Section 4.2, a more accurate LCOE was computed for our final SUMR-13C design in order to carefully validate the LCOE reduction achieved. This will be discussed further in Section 5.3.

4.3. A walk through a single design iteration

In a single design iteration, aimed at reducing the LCOE of wind energy, we first target increases in power capture (AEP) through larger rotor sizes, and then seek reductions in capital expenses ($CapEx$) by minimizing blade mass. These objectives must be reached while satisfying realistic constraints on wind turbine operation, e.g., generator speed regulation and on the blade structure, e.g., fatigue. A single iteration of our co-design procedure, highlighting the interaction between design teams, is shown in Figure 8. In the traditional wind turbine design process, the aerodynamical design is usually followed by the structural design, and controller design is done after the wind turbine is designed. However, a well-tuned controller can enable the elimination of excessive mass in the structural design. In the traditional wind turbine design process, often a previous controller (that is not tuned for the new rotor design) is used during the structural design. By tuning the controller for the new rotor before the structural design, and by incorporating the feedback loops indicated in Figure 8, each rotor design iteration process along with the feedback loops shown in Figure 5 lead to an iterative sequential co-design procedure that enabled us to design a SUMR-13 turbine to achieve 25% reduction in LCOE relative to the CONR-13 as will be discussed below.

Since rotor geometry has the greatest effect on power capture and blade loads, aerodynamic design begins with

results from closed-loop simulations, particularly power capture and blade moments at rated wind speed. Aerodynamic design is performed using the design tools PROPID and PROFOIL [42, 43]. PROPID is an inverse design tool that solves for the rotor geometry, given desired performance specifications like power, tip-speed ratio, axial induction, airfoils used, and desired lift coefficient distributions. PROFOIL is used for airfoil design; it is also an inverse design tool which allows for the design of airfoils given prescribed velocity distributions, geometric constraints (thickness and camber), and aerodynamic properties (moments). The rotor definition is then converted into input files that can be used in aeroelastic simulation codes such as FAST [34].

Control system design begins by using the aerodynamic definition of the rotor and the approximate structural properties of the blade, which can be estimated using scaling methods, e.g. [44, 45]. Quasi-steady simulations are performed in FAST, which simulate the turbine across the operating region with a wind shear indicative of the offshore location for which the turbine is sited; these simulations provide estimates for AEP and structural loads. If there is adequate AEP, the controller will be fully tuned for operation. We use an industry-standard control architecture [25, 35], which uses a lookup table to implement the desired (aerodynamically specified) power control in below-rated wind conditions and a gain-scheduled proportional-integral control in above-rated conditions to regulate generator speed. The parameters of the controller are tuned so that peak blade loads are minimized and no operational DLC wind environment results in a generator speed that is 20% greater than rated [46]. Using blade mass and load estimates, edgewise and flapwise blade stiffness targets are computed to satisfy strain limits; these are used as a starting point for structural design. If during structural layup design (described next), these mass and stiffness distributions change significantly, the controller is re-tuned. While controller tuning (for below-rated, above-rated, and the transition operating region) may require up to a week when done manually in conjunction with

aero-elastic computer simulations; automating the tuning procedure [46, 47] reduces the controller design time to a few hours on a normal desktop computer; this expedites the co-design process to explore more of the design space.

The detailed structural design layup is performed in Nu-MAD [48], where the composite structure at each spanwise location along the blade is defined by a stack of materials. The amounts of materials are optimized in order to minimize blade mass, which impacts $CapEx$. However, the blade is subject to structural constraints such as [49]:

- Material strains: The strain limit at each layer and spanwise location can not exceed its prescribed value.

- Tip deflection: The allowable deflection that the blade can experience is defined based on its clearance from the tower.

- Fatigue: The blade must survive for 20 years while being subjected to cyclic loads and turbulent loads during its operational lifetime.

- Buckling: The individual composite panels must be able to withstand compressive loads to avoid excessive out-of-plane deformations.

- Dynamic and flutter stability: The blade natural frequencies are to be designed to avoid resonance with the wind turbine. Flutter stability for long blades are designed to be above the operational envelope of the turbine [50, 51]. The flutter stability boundaries of the blade are computed by carrying out an eigen analysis of the aeroelastic system including structural dynamics and aerodynamics constructed using Theodorsen unsteady aerodynamic theory; details regarding the method are presented in [50].

Individual research teams usually focus on methods for improving their own design processes. However, in an integrated design like the one described in this article, each team must change its typical approach.

4.3.1. Modified aerodynamic design

Apart from using the inverse design methodologies (PROFOIL and PROPID) for the airfoils and blade shape (outer mold line) as already described, the aerodynamic design of the rotor when using an integrated co-design approach differs from the more common traditional approach primarily in three ways:

First, a typical rotor aerodynamic design begins with requirements on rotor rated power, tip-speed ratio, average and rated wind speeds, and structural geometric requirements for the blade airfoil thickness distribution. These data are then used to select a family of airfoils to begin the blade design – chord, twist, pitch, and distribution of airfoils along the blade. However, in the integrated co-design approach, the structural design and aerodynamic design

(both airfoils and blade geometry) were more closely coupled and iterative by way of PROFOIL and PROPID, leading to many unique design iterations being evaluated in FAST with corresponding controller iterations.

Second, it is well known that to achieve a maximum rotor power coefficient, $C_{p_{\max}}$, the axial induction factor should be a constant value of 1/3, which is defined by the Betz limit in momentum theory [52]. However, in this study, it was found that lower axial induction rotors (with axial induction factor less than 1/3) yields lower LCOE as compared with those corresponding to the Betz-limit based aerodynamically optimum rotors. The correspondingly lower LCOE mainly results from lower blade loads and consequently lower blade weights thereby lowering costs even though the lower axial induction requires longer blades (more swept area) to achieve the fixed/prescribed rated power (13.2 MW). Thus, while the resulting blades do not lead to the aerodynamically optimal power coefficient $C_{p_{\max}}$, they are superior to traditionally designed rotors as measured by LCOE.

Third, the aerodynamic design of the rotor evolved across iterations with both the structures and controls teams until a final design was realized. More typically in the overall design process, the controller is developed long after the aerodynamic design has fully matured. By incorporating the feedback loop between the controller design and the aerodynamic design blocks in Figure 8, the aerodynamic designs could be adjusted to ensure that the power and AEP goals of the rotor design are achieved. Thus aero-structural-control co-design was leveraged in the design of the SUMR 13 MW rotor.

4.3.2. Modified control design

In a typical wind turbine design, the control system is designed and fine-tuned only after the aerodynamic and structural definition of the rotor is determined. Controller tuning is usually the final step in the overall design and can be a lengthy process. Recent research in wind turbine control reflects this process [35]; control schemes are designed and tested on a fixed model with the goal of reducing structural loads. Arguments are then made that the control scheme will increase turbine lifetime or mitigate problems when turbines are deployed in the field. In contrast, by applying load-reducing control schemes using preliminary structural sizing before detailed structural design, load-reducing control can enable

- lighter blades through reduced design loads, or

- longer blades that are still structurally feasible.

For control design to occur during the design phase of a rotor, the process must be expedited. The controller tuning process typically requires the selection of dozens of parameters that ensure safe operation and the desired power production, while also minimizing structural loads.

We have automated the controller design process by reducing the set of parameters necessary for controller tuning so that a rotor can be tuned for operational DLCs in

a few hours [46, 47]. Engineers typically use experience-based rules-of-thumb for tuning the parameters that influence the closed-loop behavior of the rotor speed controller. We have developed an automated and optimized tuning procedure to ensure we are properly comparing turbine models. We constrain the architecture of the controller, using a standard scheme found in the literature [25]. The generator torque is controlled using the standard control law

$$\tau_g = k\omega_g^2, \tag{9}$$

where τ_g is the generator torque, ω_g is the generator speed, and k is the optimal control gain, which depends on rotor properties. Linear transition regions are used to control the torque between cut-in and rated wind speeds [25].

The pitch controller is a gain-scheduled proportional-integral (PI) controller, the standard basis of several research controllers [53, 36]. A detailed description of the automatic and optimal tuning process is described in [46], and we will summarize it here. Turbine linearizations are performed to determine the gain scheduling parameters, and DLC simulations are used to fine tune the regulator mode of the pitch controller. The regulator mode (parameterized by its natural frequency and damping ratio) determines the PI gains of the pitch controller and how quickly the turbine reacts to disturbances in the wind. A fast response, with a high natural frequency, regulates generator speed best, but also results in larger thrust-based loading on the blades and tower because of the increased pitch actuation. For each SUMR turbine, the model was fixed and our control goal is to reduce peak blade flapwise loading and constrain the maximum generator speed. Using the worst case DLC, simulation results can be used to estimate the gradient of the cost function (peak blade flapwise loading with a penalty on the maximum generator speed) and iterate to find the optimal set of pitch control gains for each rotor [46].

Because we optimized the controller for each turbine design, we could be sure that we were using the best tuned "standard" controller for our design goals. Each closed-loop system then performed well in terms of power capture and blade flapwise loading, and fair comparisons between wind turbine designs could be made.

4.3.3. Modified structural design

Traditionally, an initial rotor design is established by upscaling an existing design definition of a wind turbine that meets the various design requirements. This initial design, along with a baseline controller, is used to simulate a set of DLCs as prescribed by the IEC to determine the driving load case for the structural design. Using this load case, a detailed structural layup is modeled for the aerodynamic geometry of the blade with tools like NuMAD [48]. Further, these designs are iterated over to reduce blade mass as well as meet constraints including material strain, tip deflection, fatigue life, buckling, and structural dynamics that are set forth by standards like IEC and GL [4, 5].

To be able to iterate on multiple designs and meet a target of 25% reduction of LCOE within an aggressive time schedule, the design process had to be leaner and faster for SUMR-13. For an initial design, traditional scaling laws were used to determine the desired flapwise, edgewise, and torsional stiffnesses to satisfy a subset of the design requirements (maximum strain and maximum tip deflection). These stiffness distributions are used as a reference to later build detailed layups while trying to minimize the cost of the blade. After a satisfactory initial design is achieved, the baseline controller is updated using the new mass and stiffness distribution, and the AEP is also evaluated since it is affected by tip deflection. When the difference between two designs is lower than a predetermined threshold, and dynamic stability and flutter performance of the blade are satisfied, more computationally expensive calculations like buckling and fatigue life are performed and updates are made in the structural layup to meet all the constraints.

The design is finalized by ensuring that the layup is feasible and manufacturable. The model of the blade is then shared with the controls team for further controller tuning and determination of the final turbine parameters.

5. SUMR-13 designs

In this section, we apply the aerodynamic-structural-control co-design process outlined in the previous section and describe the three major iterations (see Table 2) that led to a SUMR-13 design that achieves a 25% LCOE reduction relative to the CONR-13.

5.1. SUMR-13A: 25% less rotor mass relative to CONR-13

The baseline rotor for CONR-13 is a 3-bladed upwind rotor configuration, with a total rotor blade mass of 148,557 kg (49,519 kg per 100-meter CONR-13 blade). As noted, CONR-13 was designed through an integrated aero-structural co-design process where the aerodynamics and structural performance were optimized together [17]. Because the SUMR concept is new, the design process began with an initial trade study that examined aerodynamic and structural trade-offs in a sequential process. Multiple aerodynamic definitions were considered, all with blade lengths of approximately 100 meters; however, the chord size (length of the cross section of the blade) was varied in each design [18]. For each aerodynamic design, sizing of the composite structure and structural load checks were performed. It was determined that the initially selected large chord design was difficult to optimize for mass, so one of the smaller chord designs was selected for further optimization, which provided the ability to reduce the mass of the rotor blade set by over 25% [22]. While the initial aero-structural optimization was already fruitful, the load reduction achieved via new controllers for both extreme event and fatigue loads provided ability to further reduce

Table 2: Summary of major characteristics for conventional CONR-13 and sequence of three SUMR-13 wind turbine designs.

Turbine Model	CONR-13	SUMR-13A	SUMR-13B	SUMR-13C
Rated Power	13.2 MW	13.2 MW	13.2 MW	13.2 MW
Rated Rotor Speed	7.44 rpm	9.90 rpm	7.99 rpm	6.87 rpm
Hub Height	142.4 m	142.4 m	142.4 m	168 m
Num. Blades	3	2	2	2
Blade Length	100.5 m	98.7 m	122.9 m	143.4 m
Max Chord	5.23 m	7.50 m	6.79 m	9.29 m
Rotor Position	Upwind	Downwind	Downwind	Downwind
Cone Angle*	$-2.5°$	$5°$	$12.5°$	$12.5°$
Capacity Factor[†]	47.0%	47.9%	51.2%	63.4%
Blade Mass	49.5 Mg	54.3 Mg	101.8 Mg	107.7 Mg

Environmental Parameters	
Wind Turbine Site Class	Class IIB[‡]
Cut-in, cut-out wind speed[§]	3, 25 m/s
Mean wind speed at 50 m, hub height	7.87, 9.11 m/s
Weibull shape, scale factor	2.17, 10.3

*Cone angles are negative for upwind rotors and positive for downwind rotors.

[†]The capacity factor represents the percentage of actual electrical energy output over a given period of time relative to the maximum possible electrical energy output over that period.

[‡]Class IIB winds average 8.5 m/s at hub height and have turbulence intensities of 16% [4].

[§]Wind turbines are designed to operate between the cut-in and cut-out wind speeds [35, 52]; these are often also design parameters.

material usage and lower the blade mass. We refer to this initial 13.2 MW rated SUMR rotor as the SUMR-13A rotor. SUMR-13A achieved a mass reduction of just over 25% in the rotor for the 2-bladed downwind configuration, compared to the CONR-13. Since the same materials were used to design SUMR-13A and CONR-13, the rotor cost for SUMR-13A was also reduced by approximately 25% relative to that of CONR-13.

5.2. Trade studies leading to SUMR-13B

After evaluating the LCOE of the SUMR-13A wind turbine, we found that blade mass has a relatively small effect on the overall $CapEx$: a 25% decrease in total rotor cost will only result in about a 3% decrease in the overall $CapEx$ (Figure 12(b)). This is because the rotor cost is only a portion of the wind turbine $CapEx$, which also includes the tower and nacelle. Further, the wind turbine $CapEx$ is only approximately one third of the overall $CapEx$ (Figure 7). In order to reach our goal of reducing the LCOE by 25%, we turned our attention to increasing AEP. To increase AEP, more power must be captured by increasing rotor size. Increasing rotor size increases $CapEx$ slightly, but we can still achieve lower LCOE because the AEP increases much more significantly as the rotor size increases.

Larger rotors result in heavier blades (Figure 3) and a larger thrust force, which increases structural loading on all the wind turbine component parts, from the blades to the tower base. To understand how model changes impact the structural loads and power capture, we developed a model that uses a reduced number of FAST simulations to estimate fatigue and extreme loads on wind turbine components [54, 55]. Instead of 120 ten-minute simulations for DLCs 1.2 and 1.3 (using 6 random turbulent seeds at 10 different mean wind speeds across the wind turbine operating range for each DLC), we can estimate design driving load cases using 40 three-minute simulations, which allows us to estimate the design load for a large number of rotor design iterations more rapidly. In our study, we evaluated [55]

- blade loading due to aerodynamic and structural effects,

- main bearing loading, considering the number of blades, teeter, downwind coning, and the use of individual pitch control,

- yaw bearing loads considering the nacelle center of mass and rotor overhang, and

- tower loads considering the number of blades, cone angle, and rotor axial induction.

To analyze design trade-offs without performing DLC simulations for every parameter change, we developed a harmonic load model. The harmonic load model is based on the idea that design loads (computed in a turbulent environment) for large rotors can be estimated by the loading only due to wind shear and gravity.
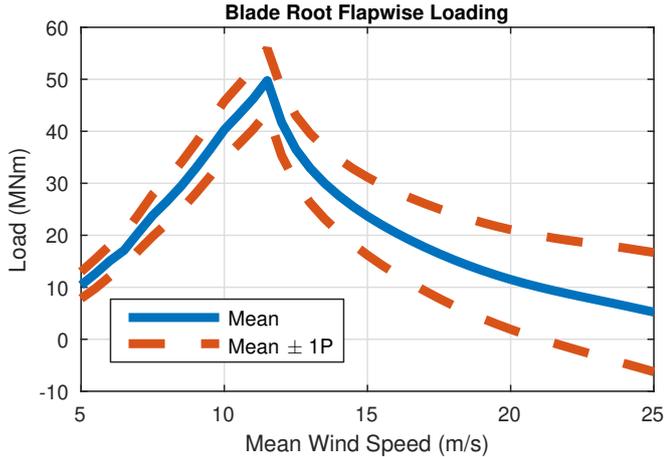
Figure 9: An example of the mean and 1P load component of the blade flapwise load of the SUMR-13A, which was used to estimate the peak and fatigue loading of the rotor.
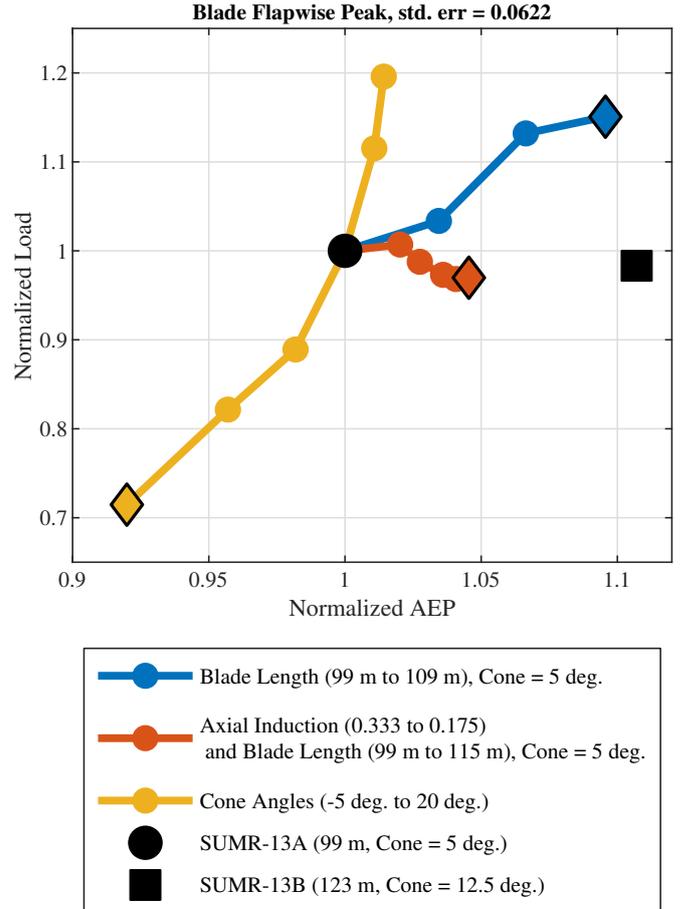

Figure 10: Trade-offs between power capture and peak blade load for the aerodynamic design studies, where blade length, axial induction, and cone angle were varied. Each dot represents a rotor design (evaluated with the simplified harmonic load mapping estimate [55]), and each line represents a design study. Results are normalized to those for the SUMR-13A. The SUMR-13A is designated by the black circle at (1,1), and each diamond represents the maximum deviation for each trade study. The SUMR-13A and SUMR-13B are detailed wind turbine designs evaluated using the full set of DLC simulations.

We simulate each turbine model across operational wind speeds with constant wind, exponential shear, and all of the degrees-of-freedom enabled. From these simulations, we compute the harmonics (1P (once per revolution) to 4P) of each load signal. The dominant harmonic (1P for blade loading) is then superimposed with the mean load (0P, blue) across wind speeds, resulting in a "load profile" for each moment direction, as shown in Figure 9 for the SUMR-13A for the blade root flapwise load. From these load profiles, peak and fatigue harmonic loads (and power) are computed [55], which provides a qualitative indication of where loads are problematic in the operating wind speeds and can also be used to compare rotor designs.

If a subset of the design studies is simulated using the full set of DLCs, a mapping from the harmonic loads to the DLC loads can be derived. The mapping provides design load estimates, or quantitative information about the design changes, that have less than 12% residual error with the DLC-simulated loads [55]. In the following, we provide a summary of the results from the design studies.

We first evaluated the effect that aerodynamic changes have on blade loads and power capture, and Figure 10 summarizes the results. The SUMR-13A is used as a baseline for comparison and all rotors have a rated generator power of 13.2 MW. To increase the available rotor power at 11.3 m/s, the rated wind speed of the SUMR-13A, the blade length was increased. A 10 m increase in blade length results in a 9.6% increase in AEP and a 15% increase in peak blade flapwise load (blue curve in Figure 10). As detailed in [55] and illustrated by the red curve in Figure 10, decreasing the axial induction while simultaneously increasing the blade length such that peak blade loads do not increase, can lead to increased power capture. By constraining the thrust load in PROPID and allowing chord and blade length to be free variables, a longer (by 16 m), more slender blade captures more power (4.5% increase) while constraining peak loads. The effect of con-

ing (yellow curve in Figure 10) was evaluated by varying the cone angle of the SUMR-13A from $-5°$ (upwind) to $20°$ (downwind). Downwind coning at $20°$ reduces AEP slightly (8%), but peak loads are decreased significantly (29%), compared to the $5°$ of cone angle of the SUMR-13A (Table 2). Compared with the design trade-off associated with increasing blade length, increasing the cone angle decreases loads faster than blade length increases them; this effect highlights why large downwind cone angles are attractive for large rotors.

In general, changes that increase or decrease structural loading will increase or decrease power capture, respectively. When evaluating these design studies, our goal is to maximize power and minimize structural loads, and hence we aim to achieve results in the bottom right quadrant of Figure 10. The effect of each individual trade study (change in load, change in power) approximately sum when combining changes to the rotor. This is illus-

trated by the SUMR-13B design choice in Figure 10. Starting from the SUMR-13A, the blade length is increased to the maximum of the blade length study (blue diamond), the axial induction is decreased to 0.2 (with corresponding further increase in blade length), and the cone angle is increased from 5° to 12.5°, resulting in the approximate power capture and peak load of the SUMR-13B. Compared to the SUMR-13A, the SUMR-13B blade is nearly 25% longer (Table 2) and captures 11% more power (Figure 10), but is 87% more massive (Table 2). The increased power capture and hence increased AEP (Figure 12(c)) reduces the LCOE significantly (Figure 12(d)) compared to the slight LCOE increase due to the increase in $CapEx$ (Figure 12(b)) from the greater blade mass.

Our goal when designing the SUMR-13B was to constrain peak blade flapwise loads and increase the AEP; we achieved this, but it was not possible to constrain the loads on all the turbine components. One negative effect of increasing blade length is the increase in edgewise (in-plane) fatigue loads due to increased blade mass. Compared with the SUMR-13A, the SUMR-13B increases these loads by up to 100%, depending on the designed blade mass and stiffness. Increases in edgewise fatigue must be accounted for by increasing the edgewise stiffness through trailing edge and leading edge reinforcement. Additional reinforcement has additional mass, which then contributes to more edgewise fatigue. This design feedback system does result in a feasible solution for blade mass, stiffness, and edgewise fatigue: the load increases 82%, mass increases by 87%, and edgewise stiffness increases by 124%, compared to the SUMR-13A [55].

The additional mass associated with enlarged rotors transfers to the non-rotating components of the turbine. The lack of rotor symmetry (compared to a 3-bladed rotor) and a downwind rotor center-of-mass contribute to large peak and fatigue loading on the main bearing in the SUMR designs. Two-bladed rotors have this issue because the moment about the tilt axis (due to wind shear) when the blades are vertically oriented is not equal to the moment (due to gravity) when the blades are horizontally oriented; these loads are equal in three-bladed rotors [55]. We found that 2-bladed rotors have a 22% greater damage equivalent load (DEL: essentially, strain-stress cycle counting [56, 57]) on the main bearing, compared to 3-bladed rotors with the same blades. These cyclic loads in the non-rotating frame transfer to the yaw bearing and tower base, increasing fatigue on each component. To an extent, individual pitch control and proper teeter design can alleviate these effects, which change the loading on the blades at different blade locations and reduce the combined effect of these loads at the rotor hub; further details showing the effect of a teetering rotor on loads can be found in [55]. If used during turbine development, this is another potential benefit of including control design in the co-design process [55].

When considering massive, downwind rotors, the peak main bearing load is the most problematic load compo-

nent. A downwind 2-bladed rotor with a 5° cone angle experiences only 15% greater peak main bearing loads than an upwind 2-bladed rotor with a −5° cone angle. However, 3-bladed rotors have lower peak main bearing loads than 2-bladed rotors and coupled with increases in mass and downwind cone angle, the SUMR-13B has a +260% increase in peak main bearing load compared to the CONR-13 [55].

Main bearing loads transfer to the other non-rotating components, like the yaw bearing and tower base. Yaw bearing fatigue loads closely mirror those of the main bearing, but peak yaw bearing loads can be mitigated by reducing the rotor overhang. This is possible as downwind rotors do not require as large an overhang to avoid tower strikes compared with upwind turbines. Once the nacelle is properly balanced, both yaw bearing and tower base peak loads are reduced for downwind rotors because the blades deflect downwind and reduce rotor swept area and hence rotor thrust.

Tower fatigue, however, could be problematic for 2-bladed turbines. In order to reduce the mass (and thus the cost) of the tower, offshore towers are typically designed to be "soft-stiff," with natural frequencies between the 1P and 3P rotor frequencies. Since a 2-bladed rotor will excite the tower at 2P, significant fatigue damage is expected without a tower re-design. We designed a speed avoidance controller [55] to bypass this natural frequency, but the results still show a significant increase (+370%) in side-to-side fatigue loads at the tower base for 2-bladed rotors when compared with 3-bladed rotors. Another option is to use an even less massive "soft-soft" tower design or a floating platform, with a natural frequency much lower than the 1P rotor frequency, but this introduces a coupling of the speed controller with the tower design. While outside the scope of our project, it is an interesting application of controller co-design and is an area for future work. These design studies highlight the additional challenges associated with 2-bladed rotors, the SUMR concept, and increases in rotor size.

5.3. SUMR-13C: Achieving 25% LCOE reduction

When designing the SUMR-13A and SUMR-13B, we found that the energy capture (AEP) had the most significant effect on the cost of energy, while changes in blade cost and resulting $CapEx$ were relatively small. When analyzing the loading on the SUMR-13B rotor, we found that edgewise blade loads would likely drive blade design when blade lengths exceed 110 m. Our goal for the SUMR-13C rotor was to design a rotor with blades that survive the DLCs in Table 1 and reduce the cost of energy by 25%, compared to the CONR-13. Given our previous findings, we aimed to achieve this primarily through AEP increases.

We continued to carry out trade studies, now relative to SUMR-13B, with resulting figures similar to that shown in Figure 10. We iterated on these trade studies and selection of next best parameters (coning angle, blade length, axial induction factor) with which to carry out another detailed
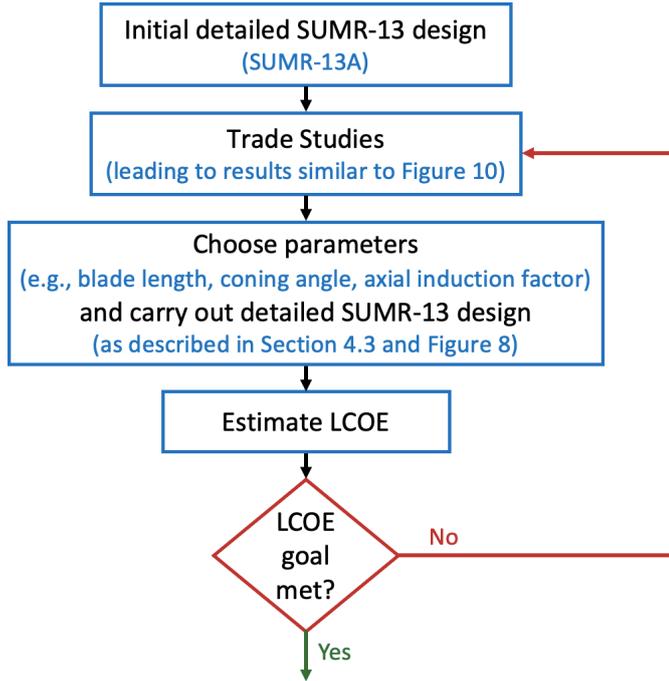
Figure 11: We iterated through trade studies to choose parameters for each detailed SUMR-13 design until we achieved our LCOE goal.
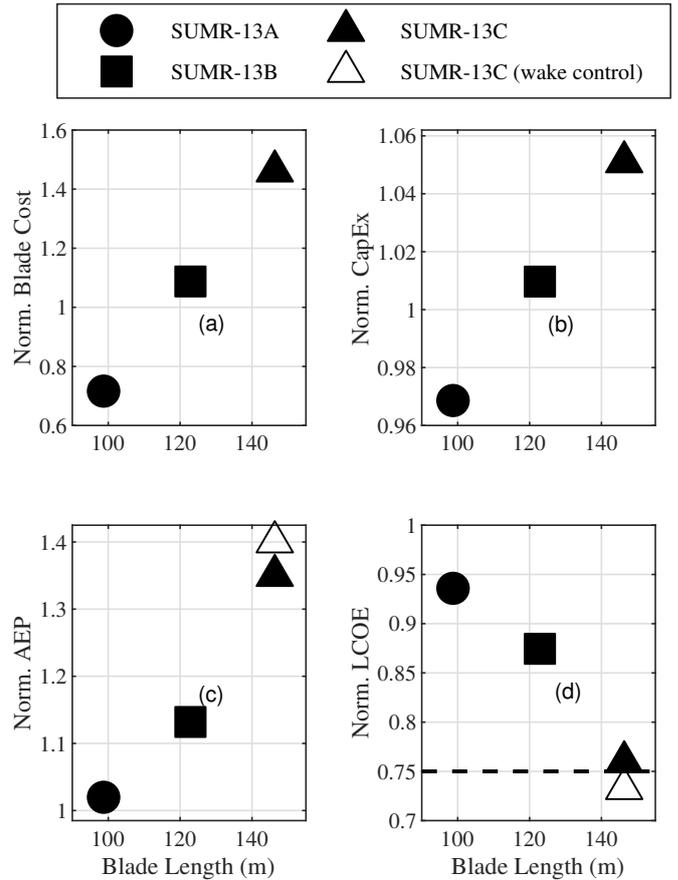

Figure 12: These plots show the impact of blade length for a 13 MW two-bladed downwind rotor relative to a conventional upwind 3-bladed rotor on (a) blade cost, (b) capital expenditures ($CapEx$), (c) annual energy produced (AEP), and (d) levelized cost of energy (LCOE). All results are normalized relative to the CONR-13. Additional wind farm wake control effects were explored for the SUMR-13C, where further benefits in AEP and LCOE can be achieved with downwind turbines.

rotor design. Within each detailed rotor design iteration, we used the process described in Section 4.3 and summarized in Figure 8. This overall procedure is diagrammed in Figure 11. We had three major detailed SUMR-13 rotor designs (A, B, C) as indicated in Table 2. However, there were many simplified turbine models evaluated (smaller dots as well as the diamonds in Figure 10) leading to choosing the next set of parameters at which to do a detailed rotor design. The number of simplified turbine models varied in each iteration, and we chose these models to try to increase AEP while also trying not to have structural loads increase too significantly. As we neared our final SUMR-13C design, we used more higher fidelity modeling and analysis to ensure that we would meet our LCOE goal and to validate the final design.

To increase our energy production, we first considered our previous work in control design, which shows that AEP can be increased by 2% when the power reference is controlled, boosting power output, while still maintaining generator speed and blade load limits [55, 58]. Next, using the harmonic model outlined in Section 5.2 and detailed in [54] to estimate the AEP, we designed and analyzed aerodynamic changes to the SUMR-13B: progressively increasing blade length from 125 m to 145 m and the axial induction factor from 0.2 to 0.225, until the combined AEP (due to aerodynamics and controls modifications) was increased by 35% compared to the CONR-13.

We estimated the blade mass by assuming a linear increase in mass with blade length (considering the previous SUMR-13A and SUMR-13B designs), which provided a sufficiently accurate initial estimate. We expected the

SUMR-13C blades to weigh 112 metric tons each, which would result in approximately a 50% increase in rotor blade mass (and cost) and a 5% increase in $CapEx$, compared to the CONR-13 (Figure 12). Later, during the structural blade design, we more accurately calculated the blade mass (Table 2) and our estimates proved to be adequate. The 35% increase in AEP along with the estimated 5% increase in $CapEx$ were expected to yield close to a 25% decrease in LCOE, but the structural blade design would determine the final mass and feasibility of the design. After the detailed structural design, the LCOE of the aero-structural-control co-designed rotor was computed based on relatively accurate cost models, and the resulting LCOE reduction relative to the CONR-13 was 24%. An additional 5% increase in AEP relative to the CONR-13 can be achieved when considering wind farm wake control effects where downwind rotors have an advantage over upwind rotors [59, 60]. A 600 MW wind farm of 45 SUMR-13C wind turbines leads to a 26.8% reduction in LCOE compared to the same wind farm with CONR-13
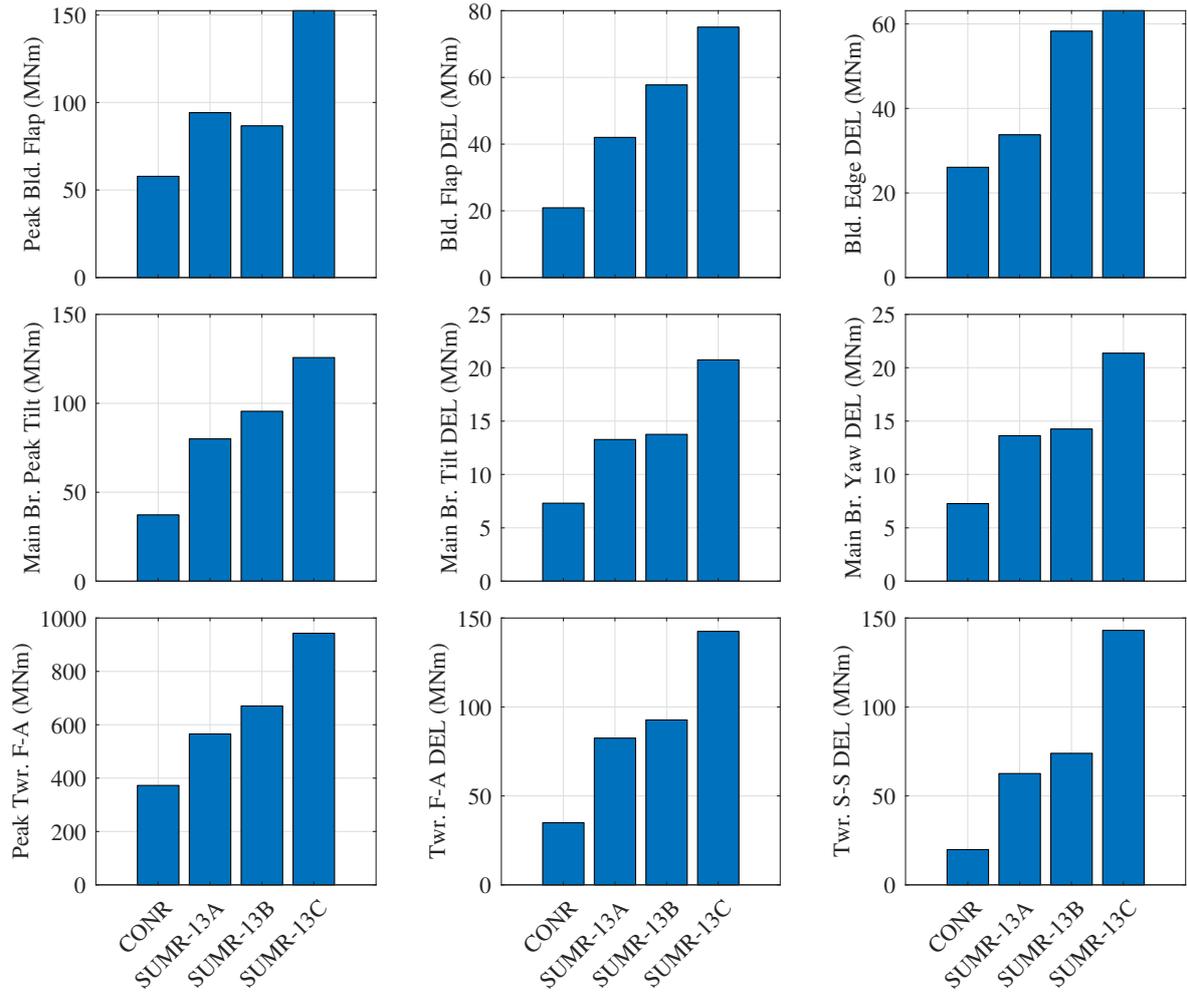
Figure 13: Blade loads (peak flapwise, flapwise damage equivalent load (DEL), and edgewise DEL), main bearing loads (peak in the tilt direction and DELs in the tilt and yaw directions), and tower loads (peak fore-aft (F-A), and DELs in the F-A and side-to-side (S-S) directions for the CONR-13, SUMR-13A, SUMR-13B, and SUMR-13C.

wind turbines (empty triangle in Figure 12(d)).

In this final design step, the structural components of the blade (e.g., the spar cap, shear web, and trailing edge reinforcement) were designed so that the blade would survive the peak loads of DLCs 1.3 to 1.5 as well as 20 years of fatigue stress determined by DLC 1.2 simulations. Ultimately, a blade was designed with a mass of 107.7 metric tons, which would achieve our LCOE goals without an additional aerodynamic re-design. Edgewise fatigue proved to be the design driving load, as expected, and reinforcement was added along the trailing edge to accommodate these stresses, resulting in a blade that is feasible with respect to the DLCs in Table 1.

Larger rotors, like the SUMR-13C will require stronger components to withstand the additional structural loading. Extreme and fatigue loads derived from the DLCs in Table 1 are shown in Figure 13. Since constraining peak flapwise loads did not reduce blade mass for the SUMR-13B, this was not the goal for the SUMR-13C. The blades of the SUMR-13C were designed with the peak and fatigue

loads in Figure 13. Of particular concern are the edgewise loads, which increase with blade mass and length. At this time, we know of no control scheme to reduce these these gravity-based loads. Main bearing loads, as discussed in Section 5.2, are particularly large for 2-bladed, downwind rotors. Tower loads also increase and the natural frequency of the tower for large 2-bladed turbines is important because the rotor must avoid the 2P frequency rather than the 3P frequency. For large turbines, soft-stiff towers (with a natural frequency less than 2P) are required, so the rotor must pass through this frequency in below-rated operation. A frequency avoidance control scheme could improve these loads significantly. While tower design was outside of the scope of this paper, this is an area for future control co-design work.

6. Conclusions and Future Outlook

We have described an aeroelastic-structural-control co-design process and illustrated how application of this pro-

cedure has led to a 13 MW novel SUMR downwind 2-bladed wind turbine design that shows 25% reductions in LCOE when compared with the traditional CONR-13 upwind 3-bladed wind turbine design. By incorporating optimally tuned controllers into the aerodynamic and structural design processes, the power production and mass reductions could be optimized to achieve the LCOE goal. The process described here resulted in a wind turbine rotor design that is significantly larger than any design to date. The final rotor diameter is almost 50% larger, yielding more than a 25% LCOE reduction, when compared to a baseline rotor (CONR-13) representative of the state of the art. Recent studies have shown that industry is indeed projected to move along this trend toward larger rotors [23], assuming that new design procedures such as our co-design process can yield feasible rotor designs.

The lower axial induction (< 0.333) SUMR-13 designs have more slender blades that are much more flexible than those of the CONR-13. For each SUMR-13 design, an integrated aero-servo-elastic model of the wind turbine was evaluated using the FAST aeroelastic simulation code [34]. The aero-servo-elastic model of the wind turbine couples the aerodynamic, structural (elastic), and control degrees of freedom. Not only is each FAST SUMR-13 model a coupled dynamics model, but it is also a coupled design model that provides a virtual design environment for modeling, simulation, and design of a wind turbine.

Although a successful design process was illustrated in this article, additional work is on-going to further improve both the control co-design process and the design tools. A new program, that started since the work described in this article was carried out, within the US Department of Energy (DOE) [61] encourages and funds control co-design approaches for designing floating offshore wind turbine technology. At the current time, the software tools available do not easily allow for simultaneous optimization of the many aerodynamic, structural, and control parameters at the level of fidelity we have considered here. The software tools (such as PROPID and PROFOIL [42, 43]) that aerodynamicists use to design wind turbine blades are not easily integrated with those (such as NuMAD [48]) that structural dynamicists use to determine the detailed structural layup of materials in the wind turbine blades and those (such as MATLAB/Simulink [62]) that control experts use to design controllers. By working more closely as a team and providing regular feedback between our groups (as indicated in Figures 5 and 8), we were able to explore more of the design space to yield the SUMR-13C design to lead to the 25% reduction in LCOE.

On-going projects such as [63] are working to advance the state of the art in software tools for control co-design of wind turbines. The envisioned tools will enable rigorous LCOE optimized designs over the lifetime (usually 20 years) of a wind turbine. Individual areas of on-going and future work include (1) refined aero-structural optimization that addresses power maximization, blade mass reduction, and rotor aero-elastic stability, (2) automatic

controller tuning [36, 46], and (3) faster detailed structural designs that provide direct input into high-fidelity models for rotor capital costs.

The 105-meter long SUMR-13 blade design that is detailed in [18] was gravo-aero-elastically scaled to 20% scale to a 21-meter long blade design [44, 45, 64, 65], and the scaled blades have been manufactured and mounted on a wind turbine platform at the U.S. National Renewable Energy Laboratory [66]. This setup is called the SUMR-Demonstrator (SUMR-D), and we ran experimental field tests with the SUMR-D from November 2019 to July 2020. The field data gathered is enabling us to better understand the performance of such highly flexible, lightweight rotor designs [67]. Based on our experimental results, improved blade structure models for highly flexible blades and models of unsteady aeroloads via tower shadow effect [68, 69]) are now being integrated into software modules and tools (such as FAST [34]) at NREL that are ultimately made freely available and will thus help to advance control co-design for wind turbines. Automatic controller tuning methods are also being integrated into these software tools [36, 46] to allow faster controller tuning which will in turn enable more wind turbine designs to be explored more efficiently. Expanding the necessary tools to fully enable control co-design for floating offshore wind turbines is an active area of research and development, and there are many avenues for future work. Several projects funded by DOE [61] are aiming to expand the control co-design approach for floating offshore wind turbines.

Our vision is that continued multi-disciplinary collaborations for wind turbine design (as well as for other complex systems) will enable better understanding of the dependencies between the aerodynamics, structural dynamics, and control algorithms. This improved understanding will lead to future co-designed wind turbines (and other systems) that will achieve higher performance and lower the cost of wind energy beyond current levels. Eventually, it may even be possible to carry out more advanced nested and simultaneous [13, 14, 15] control co-design approaches for wind turbine design.

Declaration of Competing Interest

None.

Acknowledgements

References

[1] D. Besart, Z. Finucane, B. Foley, R. Hall, R. Damiani, B. Maples, Z. Parker, A. Robertson, G. Scott, T. Stehly, F. Wendt, M. B. O. Andersen, K. Standish, K. Lee, A. Raina, K. Wetzel, W. Musial, S. Schreck, Hurricane Resilient Wind Plant Concept Study Final Report, Technical Report NREL/TP-5000-66869, National Renewable Energy Laboratory, Oct. 2016.

[2] T. Stehly, D. Heimiller, G. Scott, 2016 Cost of Wind Energy Review, Technical Report NREL/TP-6A20-70363, National Renewable Energy Laboratory, Dec. 2017.

[3] D. T. Griffith, Sandia 100-meter blade research update: SNL100-00 all-glass baseline and beyond, in: Sandia Blade Workshop, May 2012.

[4] International Electrotechnical Commission, IEC 61400-1: Wind Turbines - Part 1: Design Requirements, Technical Report, 2009.

[5] Rotor blades for wind turbines, in: Standard DNVGL-ST-0376, Dec. 2015.

[6] D. T. Griffith, The SNL100-01 blade: Carbon design studies for the Sandia 100-meter blade, Technical Report SAND2013-1178, Sandia National Laboratories, Feb. 2013.

[7] I. Arrambide, I. Zubia, A. Madariaga, Critical review of offshore wind turbine energy production and site potential assessment, Electric Power Systems Research 167 (Feb. 2019) 39–47.

[8] Ten of the biggest turbines, https://www.windpowermonthly.com/10-biggest-turbines, Sep. 2018. Accessed July 2020.

[9] GE is building the world's largest wind turbine, https://www.popularmechanics.com/science/energy/a25956533/ge-largest-wind-turbine/, Jan. 2019. Accessed July 2020.

[10] Siemens Gamesa reveals world's largest wind turbine, https://www.renewableenergyworld.com/2020/05/22/siemens-gamesa-reveals-worlds-largest-wind-turbine/, May 2020. Accessed July 2020.

[11] M. Garcia-Sanz, Control co-design: An engineering game changer, Advanced Control for Applications: Engineering and Industrial Systems 1 (Dec. 2019) e18 (10 pages).

[12] R. Patil, Z. Filipi, H. Fathy, Computationally efficient combined plant design and controller optimization using a coupling measure, J. Mechanical Design 134 (July 2012) 071008 (8 pages).

[13] J. T. Allison, T. Guo, Z. Han, Co-design of an active suspension using simultaneous dynamic optimization, J. Mechanical Design 136 (Aug. 2014) 081003 (14 pages).

[14] D. R. Herber, J. T. Allison, Nested and simultaneous solution strategies for general combined plant and control design problems, J. Mechanical Design 141 (Jan. 2019) 011402 (11 pages).

[15] H. K. Fathy, J. A. Reyer, P. Y. Papalambros, A. G. Ulsoy, On the coupling between plant and controller optimization problems, in: Proc. American Control Conf., June 2001, pp. 1864–1869.

[16] J. T. Allison, D. R. Herber, Multidisciplinary design optimization of dynamic engineering systems, AIAA Journal 52 (Apr. 2014) 691–710.

[17] D. T. Griffith, P. W. Richards, The SNL100-03 blade: Design studies with flatback airfoils for the Sandia 100-meter blade, Technical Report SAND2014-18129, Sandia National Laboratories, Sep. 2014.

[18] G. K. Ananda, S. Bansal, M. S. Selig, Aerodynamic design of the 13.2 MW SUMR-13i wind turbine rotor, in: Proc. AIAA Science and Tech. Forum & Expo., AIAA Paper 2018-0994, Jan. 2018.

[19] M. Kaminski, E. Loth, D. T. Griffith, C. Qin, Ground testing of a 1% gravo-aeroelastically scaled additively-manufactured wind turbine blade with bio-inspired structural design, Renewable Energy 148 (Apr. 2020) 639–650.

[20] C. Noyes, E. Loth, D. Martin, K. Johnson, G. Ananda, M. Selig, Extreme-scale load-aligning rotor: To hinge or not to hinge?, Applied Energy 257 (Jan. 2020) 113985 (11 pages).

[21] C. Noyes, C. Qin, E. Loth, Analytic analysis of load alignment for coning extreme-scale rotors, Wind Energy 23 (Feb. 2020) 357–369.

[22] S. Yao, D. T. Griffith, M. Chetan, Structural design and optimization of a series of 13.2 MW downwind rotors, accepted for publication in Wind Engineering (in press).

[23] M. Bolinger, E. Lantz, R. Wiser, B. Hoen, J. Rand, R. Hammond, Opportunities for and challenges to further reductions in the "specific power" rating of wind turbines installed in the United States, Wind Engineering 44 (Jan. 2020) (18 pages).

[24] V. Schorbach, P. Dalhoff, P. Gust, Teeter design for lowest extreme loads during end impacts, Wind Energy 21 (Jan. 2018) 1–14.

[25] J. Jonkman, S. Butterfield, W. Musial, G. Scott, Definition of a 5-MW reference wind turbine for offshore system development, Technical Report NREL/TP-500-38060, National Renewable Energy Laboratory, Feb. 2009.

[26] P. Jamieson, Evaluation of the coning rotor concept, Technical Report, Garrad Hassan, Bristol, England, Dec. 1996.

[27] F. Rasmussen, J. T. Petersen, P. Volund, P. Leconte, E. Szechenyi, C. Westergaard, Soft rotor design for flexible turbines, Technical Report Contract Report JOU3-CT95-0062, Riso National Laboratory, 1998.

[28] C. Crawford, The path from functional to detailed design of a coning rotor wind turbine concept, in: Proc. CDEN/C2E2 Conf., Winnipeg, Canada, 2007.

[29] S. Bansal, G. K. Ananda, M. S. Selig, Development of an aerodynamic analysis methodology for segmented ultralight morphing rotors, in: Proc. AIAA Applied Aerodynamics Conf., AIAA Paper 2017-4217, June 2017.

[30] C. Noyes, C. Qin, E. Loth, Pre-aligned downwind rotor for a 13.2 MW wind turbine, Renewable Energy 116 (Feb. 2018) 749–754.

[31] E. Loth, A. Steele, C. Qin, B. Ichter, M. Selig, P. Moriarty, Downwind pre-aligned rotors for extreme-scale wind turbines, Wind Energy 20 (July 2017) 1241–1259.

[32] B. Boukhezzar, L. Lupu, H. Siguerdidjane, M. Hand, Multivariable control strategy for variable speed, variable pitch wind turbines, Renewable Energy 32 (July 2007) 1273–1287.

[33] A. Chehouri, R. Younes, A. Ilinca, J. Perron, Review of performance optimization techniques applied to wind turbines, Applied Energy 142 (Mar. 2015) 361–388.

[34] J. M. Jonkman, M. L. Buhl, FAST User's Guide, Technical Report NREL/EL-500-38230, National Renewable Energy Laboratory, Oct. 2005.

[35] L. Y. Pao, K. E. Johnson, Control of wind turbines: Approaches, challenges, and recent developments, IEEE Control Systems Magazine 31 (Apr. 2011) 44–62.

[36] N. J. Abbas, A. D. Wright, L. Y. Pao, An update to the NREL baseline wind turbine controller, J. Physics: Conf. Series: Proc. North American Wind Energy Academy and Int. Conf. on Future Technologies in Wind Energy 1452 (Mar. 2020) 012002 (14 pages).

[37] F. Zahle, C. Tibaldi, D. R. Verelst, C. Bak, R. Bitche, J. P. A. A. Blasques, Aero-elastic optimization of a 10 MW wind turbine, in: Proc. AIAA Science and Tech. Forum & Expo., Jan. 2015.

[38] P. Bortolotti, C. L. Bottasso, A. Croce, Combined preliminary–detailed design of wind turbines, Wind Energy Science 1 (May 2016) 71–88.

[39] W. Short, D. J. Packey, T. Holt, A manual for the economic evaluation of energy efficiency and renewable energy technologies, Technical Report NREL/TP-462-5173, National Renewable Energy Laboratory, Mar. 1995.

[40] T. S. Obdam, H. Braam, L. W. M. M. Rademakers, User Guide and Model Description of ECN O&M Tool Version 4, Technical Report, Energy Research Center of the Netherlands (ECN), 2011.

[41] J. Carroll, A. McDonald, D. McMillan, Failure rate, repair time and unscheduled O&M cost analysis of offshore wind turbines, Wind Energy 19 (2016) 1107–1119.

[42] M. S. Selig, J. L. Tangler, Development and application of a multipoint inverse design method for horizontal axis wind turbines, Wind Engineering 19 (1995) 91–105.

[43] M. S. Selig, M. D. Maughmer, Multipoint inverse airfoil design method based on conformal mapping, AIAA Journal 30 (May 1992) 1162–1170.

[44] E. Loth, M. Kaminski, C. Qin, L. J. Fingersh, D. T. Griffith, Gravo-aeroelastic scaling for extreme-scale wind turbines, in: Proc. AIAA Applied Aerodynamics Conf., June 2017.

[45] M. Kaminski, E. Loth, D. S. Zalkind, L. Y. Pao, M. Selig, K. Johnson, Servo-aero-gravo-elastic (SAGE) scaling of a 13-MW downwind turbine, J. Renewable and Sustainable Energy 12 (Nov. 2020) 063301 (13 pages).

[46] D. S. Zalkind, E. Dall'Anese, L. Y. Pao, Automatic controller tuning using a zeroth-order optimization algorithm, Wind Energy Science 5 (Nov. 2020) 1579–1600.

[47] D. S. Zalkind, L. Y. Pao, D. P. Martin, K. E. Johnson, Models used for the simulation and control of a segmented ultralight morphing rotor, IFAC-PapersOnLine 50 (July 2017) 4478–4483.

[48] J. C. Berg, B. R. Resor, Numerical manufacturing and design tool (NuMAD V2.0) for wind turbine blades: User's guide, Technical Report SAND2012-7028, Sandia National Laboratories, Aug. 2012.

[49] D. T. Griffith, M. Chetan, S. Yao, Dynamics of extreme-scale wind turbines, in: Proc. Int. Modal Analysis Conf., Jan. 2019.

[50] D. T. Griffith, M. Chetan, Assessment of flutter prediction and trends in the design of large-scale wind turbine rotor blades, in: J. Physics: Conf. Series: Proc. Science of Making Torque from Wind, 2018, p. 042008 (10 pages).

[51] M. Chetan, D. T. Griffith, S. Yao, Flutter predictions in the design of extreme-scale segmented ultralight morphing rotor blades, in: Proc. AIAA Science and Tech. Forum & Expo., Jan. 2019.

[52] T. Burton, N. Jenkins, D. Sharpe, E. Bossanyi, Wind Energy Handbook, 2nd ed., Wiley, 2011.

[53] M. H. Hansen, L. C. Henriksen, Basic DTU Wind Energy controller, number 0028 in DTU Wind Energy E, DTU Wind Energy, Denmark, 2013. Contract Number: EUDP Project Light Rotor; Project Number 46-43028-Xwp3.

[54] D. S. Zalkind, L. Y. Pao, A harmonic model for loads analysis and control design of a 2-bladed wind turbine, in: Proc. AIAA Science and Tech. Forum & Expo., Jan. 2019.

[55] D. S. Zalkind, G. K. Ananda, M. Chetan, D. P. Martin, C. J. Bay, K. E. Johnson, E. Loth, D. T. Griffith, M. S. Selig, L. Y. Pao, System-level design studies for large rotors, Wind Energy Science 4 (Nov. 2019) 595–618.

[56] S. D. Downing, D. F. Socie, Simple rainflow counting algorithms, Int. J. Fatigue 4 (Jan. 1982) 31–40.

[57] H. Okamura, S. Sakai, I. Susuki, Cumulative fatigue damage under random loads, Fatigue & Fracture of Engineering Materials & Structures 1 (May 1979) 409–419.

[58] D. S. Zalkind, L. Y. Pao, Constrained wind turbine power control, in: Proc. American Control Conf., July 2019, pp. 3494–3499.

[59] J. Annoni, A. Scholbrock, M. Churchfield, P. Fleming, Evaluating tilt for wind plants, in: Proc. American Control Conf., May 2017, pp. 717–722.

[60] C. J. Bay, J. Annoni, L. A. Martinez-Tossas, L. Y. Pao, K. E. Johnson, Flow control leveraging downwind rotors for improved wind power plant operation, in: Proc. American Control Conf., July 2019, pp. 2843–2848.

[61] ARPA-E ATLANTIS (Aerodynamic Turbines Lighter and Afloat with Nautical Technologies and Integrated Servo-control) Program, `https://arpa-e.energy.gov/technologies/programs/atlantis`, August 2019. Accessed December 2020.

[62] MATLAB & Simulink, The MathWorks, Inc., 1994-2020, `https://www.mathworks.com/products/matlab.html`, accessed December 2020.

[63] Wind Energy with Integrated Servo-control (WEIS): A Toolset to Enable Controls Co-Design of Floating Offshore Wind Energy Systems, `https://arpa-e.energy.gov/technologies/projects/wind-energy-integrated-servo-control-weis-toolset-enable-controls-co-design`, January 2020. Accessed December 2020.

[64] S. Yao, D. T. Griffith, M. Chetan, C. J. Bay, R. Damiani, M. Kaminski, E. Loth, Structural design of a 1/5th scale gravo-aeroelastically scaled wind turbine demonstrator blade for field testing, in: Proc. AIAA Science and Tech. Forum & Expo., Jan. 2019.

[65] S. Yao, D. T. Griffith, M. Chetan, C. J. Bay, R. Damiani, M. Kaminski, E. Loth, A gravo-aeroelastically scaled wind turbine rotor at field-prototype scale with strict structural requirements, Renewable Energy 156 (2020) 535 – 547.

[66] C. J. Bay, R. Damiani, L. J. Fingersh, S. Hughes, M. Chetan, S. Yao, D. T. Griffith, G. K. Ananda, M. S. Selig, D. S. Zalkind, L. Y. Pao, D. Martin, K. E. Johnson, M. Kaminski, E. Loth, Design and testing of a scaled demonstrator turbine at the National Wind Technology Center, in: Proc. AIAA Science and Tech. Forum & Expo., AIAA Paper 2019-1068, Jan. 2019.

[67] M. Phadnis, D. Zalkind, L. Y. Pao, Extreme-scale wind turbine controller field validation, poster, in: American Control Conf., July 2020.

[68] C. Noyes, C. Qin, E. Loth, S. Schreck, Measurements and predictions of wind turbine tower shadow and fairing effects, J. Wind Engineering and Industrial Aerodynamics 179 (Aug. 2018) 297–307.

[69] C. Noyes, C. Qin, E. Loth, Tower shadow induced blade loads for an extreme-scale downwind turbine, Wind Energy 23 (Mar. 2020) 458–470.